Check for updates

Low loss hybrid plasmonic photonic crystal waveguide for optical communication applications

Hala Mossad I. Hassan[1] · Nihal F. F. Areed[1,2] · H. A. El-Mikati[1] ·
Mohamed Farhat O. Hameed[2,3,4] · S. S. A. Obayya[1,2]

Abstract

In this paper, a new design of hybrid plasmonic photonic crystal (PhC) waveguide is proposed and analyzed at operating wavelength of 1550 nm. The suggested design consists of hybrid cylindrical core with periodic grating as a cladding region. The effective index (n_{eff}), propagation length (L_p), and normalized mode effective area (A_{eff}) of the supported modes are numerically investigated using full vectorial finite element method. The cladding geometry is tuned to obtain long propagation length with good field confinement. The reported plasmonic PhC with uniform grating achieves long propagation length and low propagation loss of 124 μm, and 0.035 dB/μm respectively. Further, the PhC with chirped cladding offers propagation length and low propagation loss of 162 μm, and 0.0268 dB/μm at λ = 1550 nm, respectively.

Keywords Hybrid plasmonic waveguide · Surface plasmon polaritons · Photonic crystals

1 Introduction

The confinement of the light waves at the subwavelength scale beyond the diffraction limit can be realized at optical frequencies using plasmonic structures. At the optical wavelength, the metal-dielectric interfaces allow the propagation of surface electromagnetic waves. In the past few years, different kinds of plasmonic waveguides have

✉ Mohamed Farhat O. Hameed
    mfarahat@zewailcity.edu.eg

✉ S. S. A. Obayya
    sobayya@zewailcity.edu.eg

1   Department of Electronics and Communications Engineering, Faculty of Engineering, University of Mansoura, Mansoura 35516, Egypt

2   Centre for Photonics and Smart Materials, Zewail City of Science and Technology, October Gardens, 6th of October City, Giza 12578, Egypt

3   Nanotechnology and Nanoelectronics Engineering Program, Zewail City of Science and Technology, October Gardens, 6th of October City, Giza 12578, Egypt

4   Mathematics and Engineering Physics Department, Faculty of Engineering, University of Mansoura, Mansoura 35516, Egypt

been proposed such as metallic nanowires (Dickson and Lyon 2000), dielectric-loaded surface plasmonic waveguides (Heikal et al. 2013; Holmgaard and Bozhevolnyi 2007; Holmgaard et al. 2009; Weeber et al. 2017), long-range dielectric-loaded plasmonic waveguides (Hahn et al. 2015; Holmgaard et al. 2010), metal–insulator–metal (Liu et al. 2005; Pile et al. 2005), and hybrid plasmonic waveguides (Alam et al. 2010; Buckley and Berini 2007; Chelladurai et al. 2018; Güsken et al. 2019; Zenin et al. 2017). Additionally, new improvements in plasmonic waveguides have been used in realizing integrated nanophotonic devices like switches, couplers, sensors (Azzam et al 2016; Hameed and Obayya 2019), modulators (Konopsky and Alieva 2007a), Nanoantenna(Obayya et al. 2015).

In recent decade, for guiding waves with low propagation loss, hybrid modes based on the hybridization of dielectric and surface plasmon polaritons (SPPs) mode are investigated (Buckley and Berini 2007). Bloch surface wave (BSW) at the interface between truncated periodic multilayer dielectric and a surrounding media is another type of surface electromagnetic mode (Fang and Sun 2015; Wei et al. 2011). The electric field of Bloch surface polaritons (BSP) can propagate along the interface between the multilayer dielectric and the adjacent dielectric medium with a good confinement close to the surface. At certain multilayer dielectric, the BSP can be transverse electric (TE) and transverse magnetic (TM) polarizations while the SPPs are always TM polarized mode. The propagation loss of the BSP is small owing to the all-dielectric structure. Because of the electric field distribution, the BSP mode is weakly confined. Therefore, the mode confinement of the SPP waveguide is stronger than that of the BSP waveguide. Few years ago, Konopsky and Alieva (2006, 2007b) showed that a 1D photonic crystal (PhC) structure can be used around a thin metallic layer to imitate the optical properties of the structure. In this context, the coupling occurs between the SPP and the BSP modes supported by the metallic nanowire coated by 1D PhC multilayer structure, respectively. As a result, the structure has a small propagation loss with a much deeper subwavelength mode confinement. Recently, plasmonic waveguides have been studied to obtain strong confinement and low loss (Berini 2019; Güsken et al. 2019; Haffner et al. 2018; Huong et al. 2020; Liu et al. 2017; Manzoor et al. 2019; Pak and Panahi 2019; Soleimannezhad et al. 2020; Wu et al. 2020; Xu et al. 2018). In this regard, Bloch surface polaritons (Fong et al. 2017a, b; Kong et al. 2018, 2020; Wan et al. 2013) is introduced.

In this paper, a modified type of cylindrical plasmonic waveguide is proposed and analyzed, showing orders of magnitude longer propagation length than the traditional plasmonic waveguides (Chen 2010; Chowdhury 2011). The suggested structure consists of silver nano-wire embedded in SiO_2 as a core region. The core is surrounded by 1D PhC based on Si/SiO_2 (Celanovic et al. 2004; O'Sullivan et al. 2005) as a cladding region. The hybrid mode (Fong et al. 2017a; Wan et al. 2013) is generated by the coupling between the BSP mode and the plasmonic mode. The reported waveguide has advantages of using 1D PhC and plasmonic nanowire to guide the surface electromagnetic wave in a sub-wavelength scale. The effects of the structure geometrical parameters on the modal characteristics of the proposed design are investigated using full vectorial finite-element method (Obayya et al. 2000). The analyzed parameters are effective refractive index (n_{eff}), propagation length (L_p), and normalized mode area (A_{eff}). The reported designs with uniform and nonuniform grating with 10 layers show long propagation lengths of 124 μm, and 161.9 μm, respectively with low propagation loss of 0.035 dB/μm and 0.0268 dB/μm at λ = 1550 nm. The obtained propagation length is longer than those reported in Chen (2010), Chern et al. (2017), Kong et al. (2018) and Liu et al. (2015) with low propagation loss. The suggested structure could enable highly efficient light transmission in integrated photonic devices.

The paper is organized as follows. In Sect. 2, design considerations and numerical results are presented. The geometry of the proposed structure with uniform grating and their results are studied in Sect. 2.1. Further, the plasmonic PhC waveguide with non-uniform grating is introduced in Sect. 2.2 followed by the conclusion.

2 Design considerations and numerical results

2.1 Plasmonic PhC waveguide with uniform grating

The simulation results of the proposed design is made using full vectorial finite element method (FVFEM) via COMOL Multiphysics software package [https://www.comsol.com]. In order to ensure the high accuracy of the used numerical technique, a comparison was first made to validate our FVEM model. Figure 1 shows a schematic diagram of the studied plasmonic cylindrical nanowire surrounded by SiO_2 (Chowdhury 2011). In this study, silver is used with permittivity of $-129+3.3i$ (Johnson and Christy 1972; Chen 2010; Chowdhury 2011; Sun et al. 2015) at $\lambda = 1.55$ μm while the SiO_2 has permittivity of 2.25. In order to have high accuracy, high mesh is used with minimum element size of 0.45 nm and degree of freedom of 7213. Figure 1b–d show the variation of the effective index, normalized effective mode area and propagation length of the studied TM Mode with the
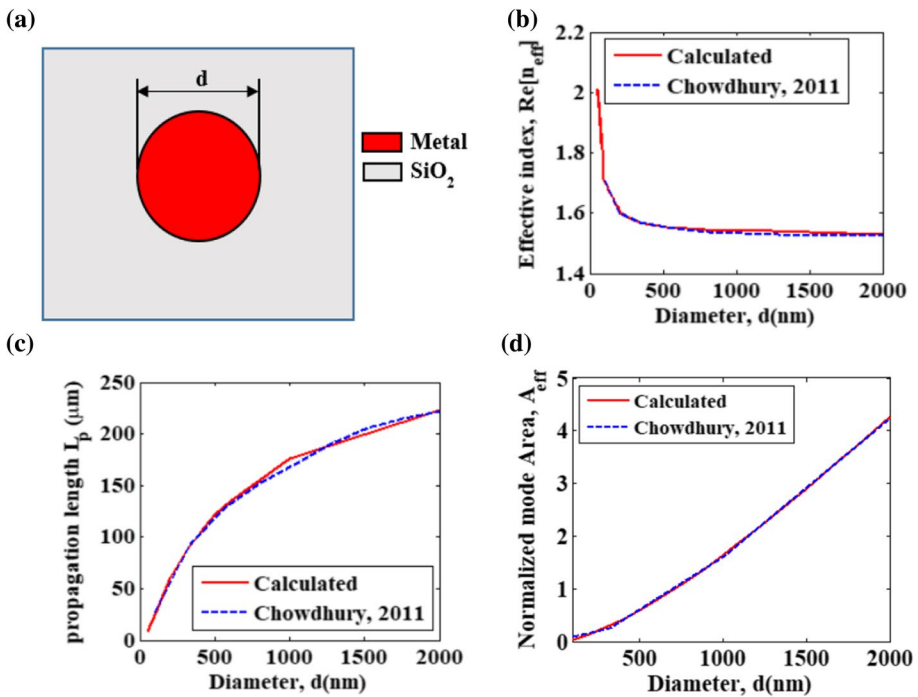

Fig. 1 **a** Schematic diagram of metallic cylinder surrounded by SiO_2 material, variation of **b** real part of the effective index n_{eff}, **c** propagation length L_p, and **d** normalized mode Area A_{eff} of the TM with the nanowire diameter d

diameter of the plasmonic cylinder. It may be seen that an excellent agreement is obtained between our results and those reported in Chowdhury (2011). This ensures the high accuracy of our calculations.

Figure 2 shows a schematic diagram of the proposed structure. The suggested design consists of a metallic wire embedded in a dielectric material surrounding by 1D PhC multilayer. The inner structure consists of a silver cylinder with a diameter d, embedded in a dielectric of silica with a thickness c. The cladding structure consists of 10 alternating Si ($\varepsilon_1 = 12.25$) and SiO$_2$ ($\varepsilon_2 = 2.25$) layers, each with thickness b. The permittivity of silver is $-129 + 3.3i$ (Chen 2010; Chowdhury 2011) at the operating wavelength of 1.55 μm. The characteristics of the proposed waveguide are studied by using finite-element method (FEM) based on COMSOL software package. In order to achieve high accuracy, minimum element of size of 1.5 nm is used with degree of freedoms of 18423. Further, first-order scattering boundary condition (Davletshin and Douplik 2016) is used to truncate the computational domain and calculate the confinement loss of the supported modes. In this study, the effective index (n_{eff}), propagation length (L_p), normalized mode area (A_1/A_0), and figure of merit (*FoM*) (Chen 2010; Chowdhury 2011) of the supported hybrid mode is investigated. It is aimed to maximize the field confinement with minimum propagation losses and long propagation length. The propagation length is calculated using:

$$L_p = \frac{\lambda}{4\pi Im(n_{eff})} \tag{1}$$

The effective mode area A_1 is obtained by Chowdhury (2011)

$$A_1 = \frac{\iint (W(r))dA}{\max(W(r))} \tag{2}$$

where $W(r)$ is the energy density taken as:

$$W(r) = \frac{1}{2}\mu_0 |H(r)|^2 + \frac{1}{2}Re\left\{\frac{d[w\varepsilon(r)]}{dw}\right\}|E(r)|^2 \tag{3}$$
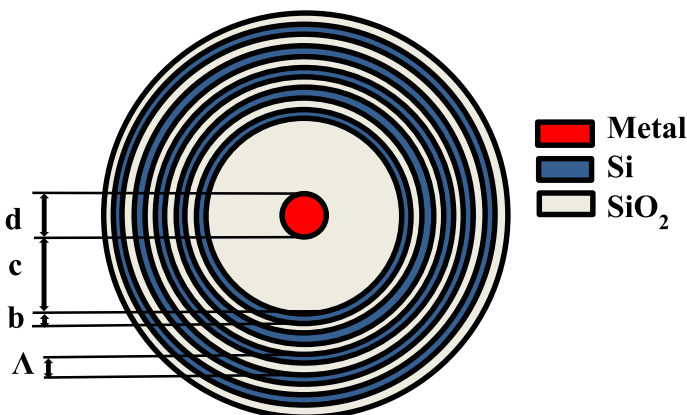

Fig. 2 Schematic diagram of the proposed hybrid plasmonic photonic crystal waveguide

where $H(r)$ and $E(r)$ are the magnetic and electric fields, respectively, μ_0 is the vacuum magnetic permeability and $\varepsilon(r)$ is the electric permittivity. In this investigation, it is aimed to maximize the FoM defined as the ratio between the normalized propagation length and normalized mode area.

$$FOM = \frac{Lp/\lambda_0}{A_1/A_0} \qquad (4)$$

where A_0 is the diffraction-limit mode area that equals to $\lambda^2/4$. The diameter of the A_g nanowire is taken by 100 nm for better optical confinement. The electric field distribution of the fundamental mode of the proposed waveguide is shown in Fig. 3. The geometrical parameter of the waveguide are initially chosen as $c = 800$ nm, $b = 24$ nm. Based on Eq. (1), the propagation length equals to 161 µm compared to 27 µm in conventional cylindrical waveguide (Chowdhury 2011) with silver cylinder.

The geometrical parameters of the proposed structure are studied to obtain strong confinement and long propagation length. First, the effect of the number of layers of the 1D PhC cladding layer is investigated. Figure 4 shows the dependences of the mode properties on the thicknesses of the dielectric layer SiO_2 for different numbers of the 1D PhC layers. Here, the thicknesses of the SiO_2 varies from 100 to 400 nm, and the number of layer of 1D photonic crystal is taken as 4, 6, 8, and 10 layers, respectively. In Fig. 4a, b, the effective index n_{eff} increases while the propagation length L_p decreases by increasing the thickness of the SiO_2. It is also evident that the reported structure has a significant improvement in the propagation length compared to conventional design (Chowdhury 2011). Further, the propagation length increase from 30 to 55 µm by increasing the number of layers from 4 to 10 layers. The result is in a good agreement with the results shown in Fig. 4c. In this
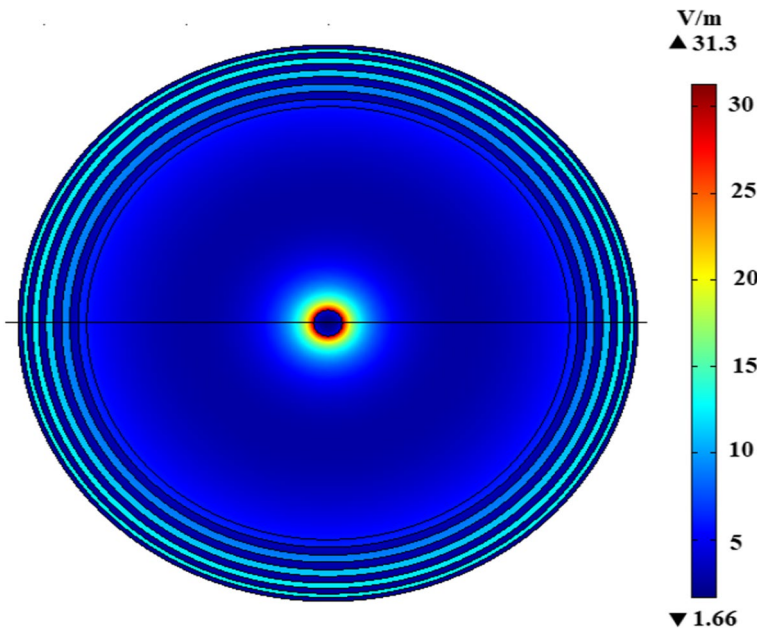

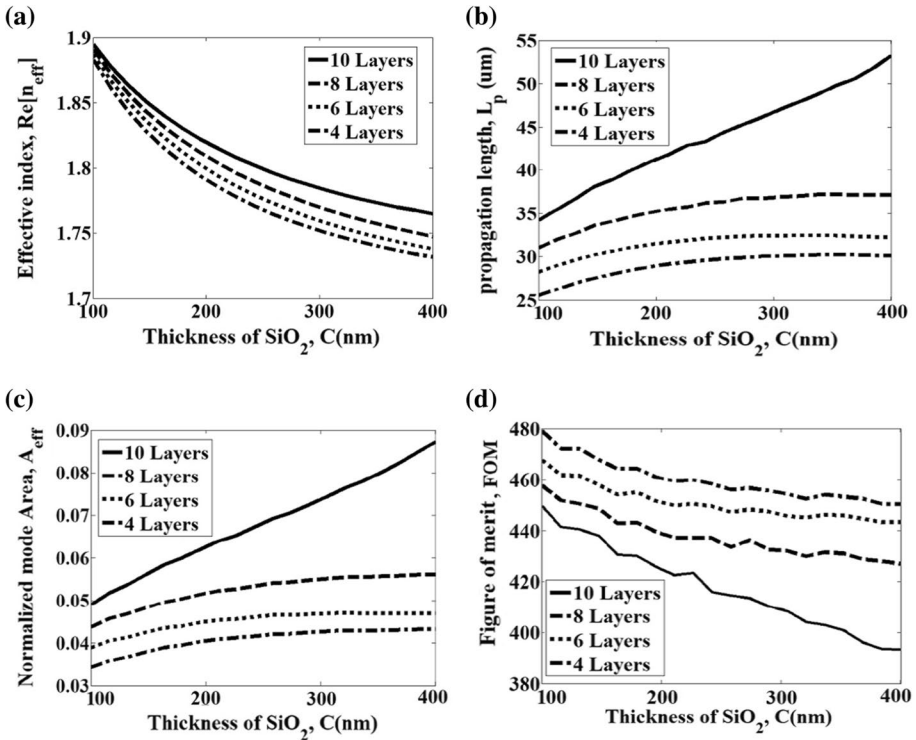**Fig. 3** Electric field distribution of the hybrid mode of the proposed design with c = 800 nm, b = 24 nm

Fig. 4 **a** Real part of the effective index n_{eff}, **b** propagation length L_p, **c** normalized mode Area A_{eff}, and **d** figure of merit FoM as functions of the thickness c of the SiO$_2$ at different N layers while $b = 20$ nm and diameter d of the A$_g$ is equal to 100 nm

context, the mode area increases with increasing the thickness *c* values. Figure 4d shows the FoM with respect to the change in the thickness of SiO$_2$. It can be noticed that the FoM decreases from 450 to 393 when the number of layer increases from 4 to 10 layers. Furthermore, the FoM of the proposed design with 10 layers, shows better performance than similar published structures (Chern et al. 2017). Therefore, 10 layers is chosen with long propagation length and good subwavelength mode confinement. However, the FoM decreases with increasing the thickness *c*. In order to prove our results, the field plots of the two dimensional (2D) electric field modes at different layers 4, 6, 8, and 10 layers are shown in Fig. 5. The field patterns at y = 0 are shown at the right of the figures. It may be seen that the optical energy is confined around the metallic nanowire. Further, the optical energy is enhanced by increasing the number of layer of 1D PhC.

In order to understand the optical performance of the uniform grating with 10 layers, the geometrical parameters effects are next investigated. The hybridization between the BSP and SPP modes can be optimized through tuning the thickness of SiO$_2$, *c* and the lattice constant $\Lambda = 2 \times b$ of the uniform grating with 10 layers. This will also enable efficient compromise between the field confinement and the propagation loss. Thickness of the lattice constant has a strong impact on the model behavior in the proposed plasmonic PhC waveguide.

Figure 6 shows the effective index n_{eff}, propagation length L_p, normalized mode area A_{eff}, and FoM of the proposed uniform grating as a function of the thickness c of SiO_2 at different values of the thickness b of the 1D PhC. Here c varies within the range 50–550 nm at $b = 10$ nm, and 20 nm. It is evident that the effective index n_{eff}, propagation length L_p, and mode area A_{eff} increase with increasing the thickness b. It may be also seen that the coupling between the metallic nanowire and the 1D PhC results in improved deep-subwavelength mode confinement where A_{eff} is lower than 10^{-2} as shown in Fig. 6c. Further, long propagation distance can be simultaneously achieved within the studied structural parameters. Figure 6d shows that the FoM at $b = 10$ nm is slightly greater than that of $b = 20$ nm. This is due to the concentration of the field in the silica dielectric layer instead of the metallic surface with reduced propagation loss.

Figure 7 shows the variation of the modal properties of the proposed waveguide with the thickness b of the 1D PhC at different values of the thickness c of the SiO_2 (200 nm, 400 nm, and 600 nm) to achieve strong interaction between the BSP mode and SPP mode with low propagation loss and subwavelength mode confinement. Here, b varies within the range 6–24 nm. Figure 7a shows an increase in the effective index n_{eff} of the hybrid mode at larger thickness of the 1D PhC b. This is due to the increase of the effective index of the BSP mode. As the thickness b increases, the propagation length (see Fig. 7b) can reach up to tens of micrometers. It is also evident from Fig. 7c that the effective area A_{eff} increases by increasing the thickness of the PhC b. Figure 7d shows the FoM as a function of the thickness of the 1D PhC b and thickness of SiO_2 c. It may be seen that the FoM decreases rapidly from 470 to around 320 by increasing b from 6 to 24 nm, which is greater than 290 that reported by Chowdhury (2011).

2.2 Plasmonic PhC waveguide with non-uniform grating

Figure 8 shows the schematic diagram of the proposed design with non-uniform grating. Similar to the first design, the structure consists of a metallic wire with a diameter d embedded in a dielectric of silica with a thickness c. The cladding structure consists of 10 alternating Si and SiO_2 layers. The effect of chirped grating is carried out based on *cos* function, *sin* function, linear function, and square function. The numerical results show that the sin function described by Eq. 5 results in longer propagation length L_p compared to that with uniform grating. As shown in Fig. 8, the chirped grating is described by:

$$\Lambda_n = \Lambda \sin(x) \text{ at } x = \left\{ \frac{\pi}{2}, \frac{5\pi}{12}, \frac{\pi}{3}, \frac{\pi}{4}, \frac{\pi}{6} \right\} \quad n = 1, 2, 3, 4, 5 \tag{5}$$

where Λ_n is the lattice constant.

Figure 9 shows the dependences of the guided fundamental mode properties on the thickness of the SiO_2 for the proposed design with uniform and chirped grating. Here c varies within the range 200–800 nm. The lattice constant $\Lambda = 2 \times b = 48$ nm for uniform grating, while the thickness of the chirped grating starts with $\Lambda_1 = 60$ nm. This indicates the dependence of the real part of the effective index n_{eff}, mode area A_{eff}, propagation length L_p, and FoM on the thickness of the dielectric layer SiO_2. Figure 9a, d show that the effective index n_{eff}, and FoM for the proposed design with chirped grating are slightly higher than those with uniform grating. It is also evident from Fig. 9b, c that the mode area A_{eff}, and propagation length L_p increase with increasing the thickness c of the SiO_2. Further, the chirped grating achieves higher A_{eff} and L_p than that of the uniform grating. This is apparently realized by leveraging the very-low-loss, high confinement properties of the BSP. In

Fig. 5 2D energy density distributions of the fundamental hybrid mode supported by the proposed wave-guide and 1D energy density distributions along y = 0 for using different layers **a** 4 layers, **b** 6 layers, **c** 8 layers, and **d** 10 layers. The other parameters are c = 100 nm, b = 20 nm, and d = 100 nm

order to prove our results, the field plots of the power density distribution of the studied mode with uniform grating and chirped grating are shown in Fig. 10 at $\lambda = 1550$. It may be seen that the energy is confined and enhanced around the circumference of the core. It is also evident from the field plots that the power density through the chirped grating has more energy concentration than that with uniform grating. Table 1 shows a comparison between the two proposed structures and those reported in the literature. It may be seen from this table that the chirped grating and uniform grating have much lower loss than the previously cylindrical plasmonic waveguide.

It is worth noting that the 1D photonic crystals have been studied and fabricated using different techniques. This includes 3D rapid prototyping (Cruz et al. 2015), digital light processing rapid prototyping (Hong et al. 2017), modified chemical vapor deposition (MCVD) (Bookey et al. 2009; Wang et al. 2018, Yang et al. 2021), and stack-and draw technique (Li and Kathirvel 2019). Further, Fink et al. (1999) have fabricated a broad-band, low-loss hollow waveguide using a LADD 30,000 evaporator fitted with a Sycon Instruments STM100 film thickness monitor. The dip coating technique is used to deposit the different layers. Also, Kuriki et al. (2004) fabricated hollow-core cylindrical photonic bandgap fibers by using thermal evaporation of an As_2Se_3 layer (2–5 μm) on each side of a free-standing 9–15-μm-thick PEI film and the subsequent 'rolling' of that coated film into a hollow multilayer tube. The plasmonic material can be infiltrated into the central hole by pumping the molten metal into the central hole at high pressure. This is because the Ag has lower melting temperature than the fiber material (silica) (Lee et al. 2008; Schmidt et al. 2008; Lee et al 2011; Tyagi et al 2010). Therefore, it is believed that the suggested plasmonic cylindrical multilayers structure can be fabricated using the current technology.

The fabrication tolerance of the proposed design is also studied to show the fabrication feasibility as shown in Table 2. The optimum geometrical parameter are chosen as $c = 800$ nm, $b = 24$ nm, $d = 100$ nm for the uniform grating while the chirped coating has $c = 800$ nm, $b = 30$ nm, $d = 100$ nm. In this study, the effect of fabrication tolerance within $\pm 5\%$ of a specific parameter is investigated while the other parameters are kept constant at their optimum values. It is worth noting that there is a tradeoff between the propagation length and field confinement. Table 2 shows the tolerance of the thickness b of the 1D PhC, the thickness c of the SiO_2, and the diameter d of silver cylinder, respectively within a tolerance of $\pm 5\%$. It may be seen from the tolerance table that the propagation length L_p, increase with increasing the studied parameters b, c, d by 5% which is desirable while the normalized mode Area A_{eff} is also increased which is undesirable effect. However, the normalized A_{eff} of the suggested design will be less than value of 4.0 that has been reported by Chowdhury (2011). Therefore, the suggested design within a tolerance of $\pm 5\%$ has a better performance than that has been obtained by Chowdhury (2011) in terms of longer propagation length and small A_{eff}.

The fiber Bragg grating is mainly used in fiber communication, fiber sensing and optical information processing. The optical fiber communication consists of many active and passive optical fiber devices. The active devices include fiber laser based on grating narrowband reflector, grating fiber amplifier to achieve flat gain and residual pumping light reflection and Ramam fiber amplifier using Bragg grating resonator. Additionally, passive devices are included in the communication systems such
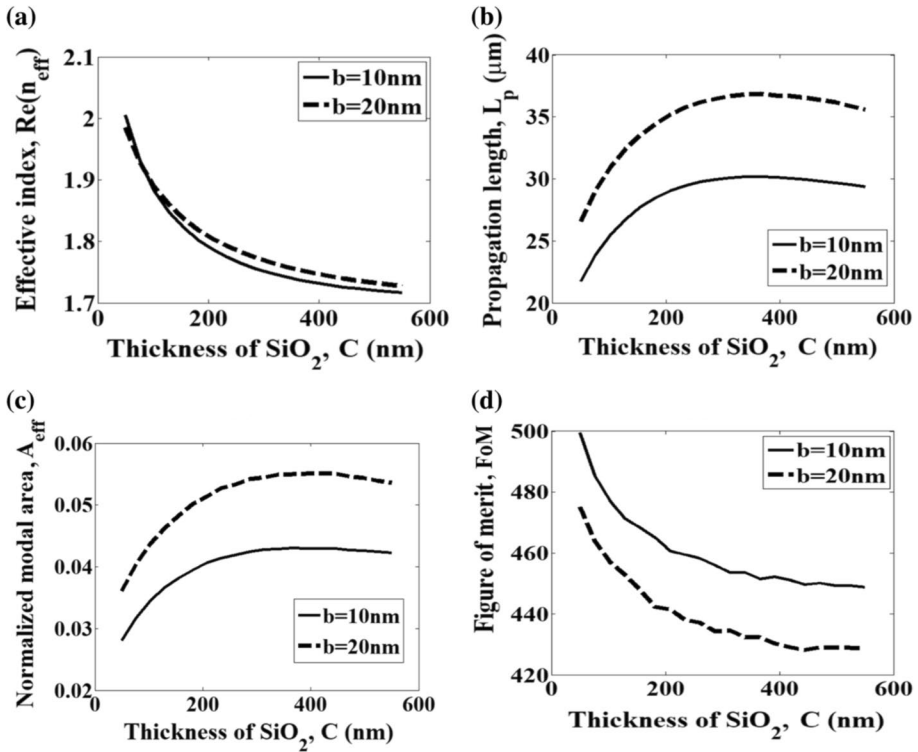
(a)

(b)

(c)

(d)
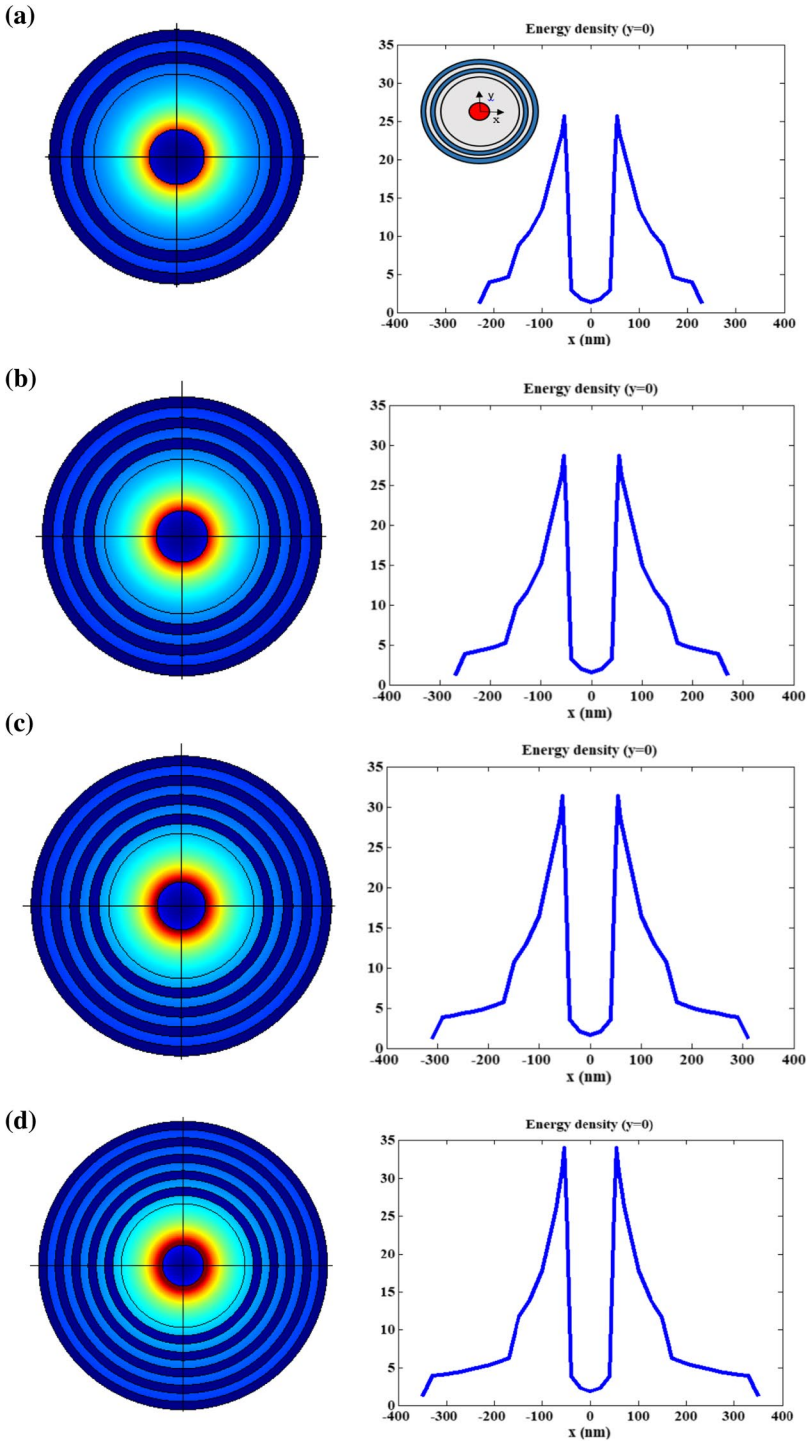
Fig. 6 **a** Real part of the effective index n_{eff}, **b** propagation length L_p, **c** modal area A_{eff}, and **d** FoM as functions of the thickness c of the SiO$_2$ at different thicknesses of the 1D PhC $b = 10$ nm, and $b = 20$ nm

as optical fiber filter, and wavelength division multiplexer (WDM) (Patki et al 2020) based on waveguide grating, dispersion compensating grating fibers and fiber sensors. In this context, fiber Bragg grating (FBG) (Othonos 1997) has been widely used in the sensing filed. Recently, plasmonic fiber sensors (Qi et al 2020) have been used with improved sensitivity. Such sensors have been used in different applications for monitoring of highways and bridges. The sensors can be developed in multi-point and distributed sensors, which relies on combination of wavelength-division multiplexing (WDM) (Luo et al 2013), time division multiplexing (TDM) (Dai et al 2009), space division multiplexing (SDM) (Gao et al 2005) and code division multiple access (CDMA) (Koo et al 1999). Further, plasmonic fiber is an important passive device in optical fiber communication. The emergence of fiber grating really realizes all-fiber filter. The FBG filter (Hunter and Minasian 1996) is an ideal device in optical communication system because of its low cost, compatibility with optical fibers and easy integration. Due to the fabrication feasibility of the FBG along with the availability of various wavelength adjustment methods, the single-channel and multi-channel wideband, high reflectivity band-stop filters and narrow-band and low-loss band-pass filters can be realized from 1520 to 1560 nm. Further, plasmonic FBG filters (Singh et al 2019) can achieve flat gain and can be used dispersion compensation and add-drop
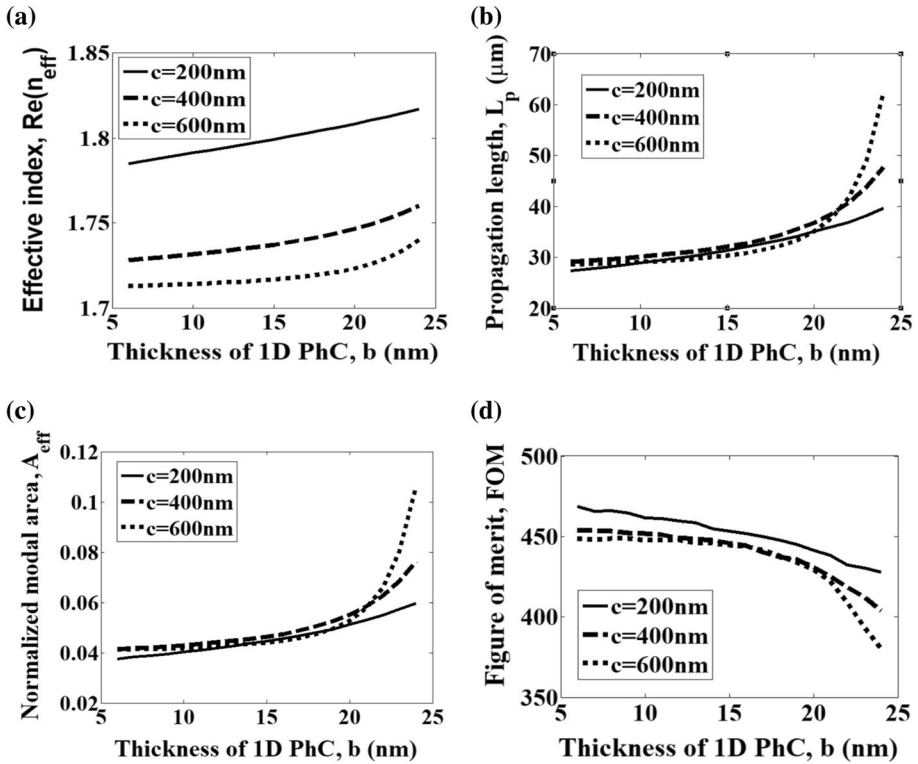
(a)

(b)

(c)

(d)

Fig. 7 **a** Real part of the effective index n_{eff}, **b** propagation length L_p, **c** modal area, and **d** FoM as functions of thickness b of the 1D PhC at different thicknesses of the SiO_2 layer; $c = 200$ nm, $c = 400$ nm, and $c = 600$ nm
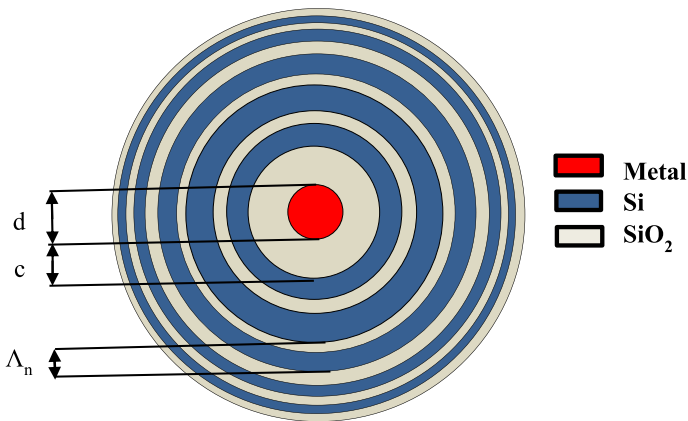

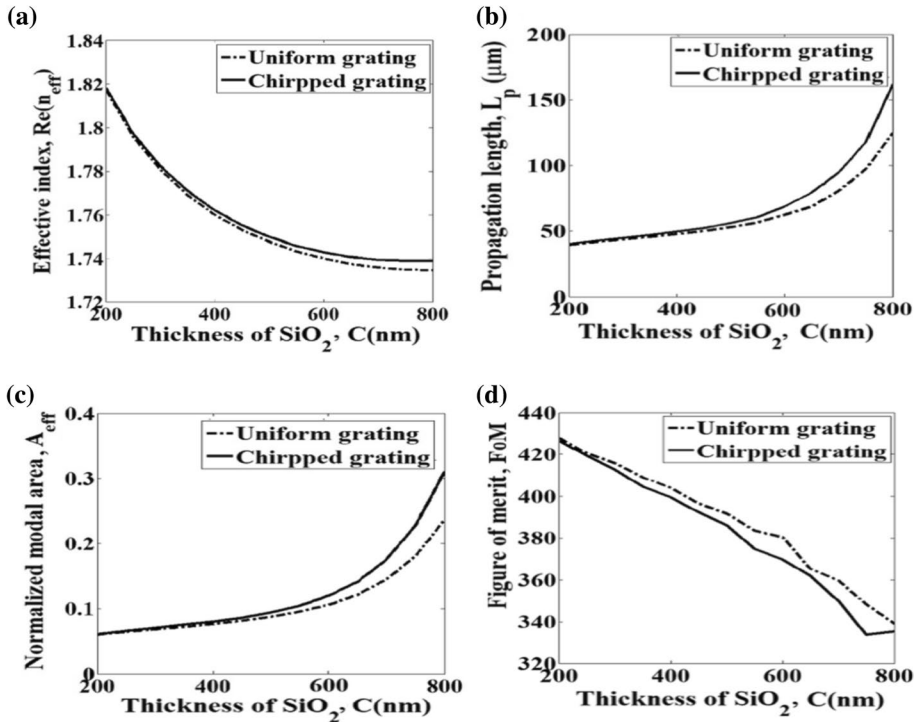**Fig. 8** Schematic diagram of the proposed design with chirped grating

(a)

(b)

(c)

(d)

Fig. 9 **a** Real part of the effective index n_{eff}, **b** propagation length L_p, **c** modal area and **d** FoM as functions of the thickness c of the SiO_2, of the proposed design with uniform grating and chirped grating

multiplexing of WDM system. Further, circular hybrid plasmonic waveguide has been reported as a fed nano-antenna that is operating at the standard telecommunication wavelength of 1550 nm (Khodadadi et al 2020).

3 Conclusion

Two cylindrical waveguides with metallic wire embedded in dielectric material are proposed and investigated. The first design has a uniform PhC grating while the second one has a chirped grating. The modal characteristics of the suggested structures are studied at telecommunications wavelength, $\lambda = 1550$ nm. By adjusting the number of the PhC layers, lattice constant, more field confinement is achieved compared to the conventional cylindrical waveguide. The reported design with uniform grating has a propagation length L_p of 124 μm and FoM of 339. However, the chirped grating achieves long propagation length L_p of 161.9 μm and FoM 335. The proposed cylindrical waveguide has the advantages of low propagation loss with suitable mode confinement, which can be used to design photonic integration with ultra-high density.
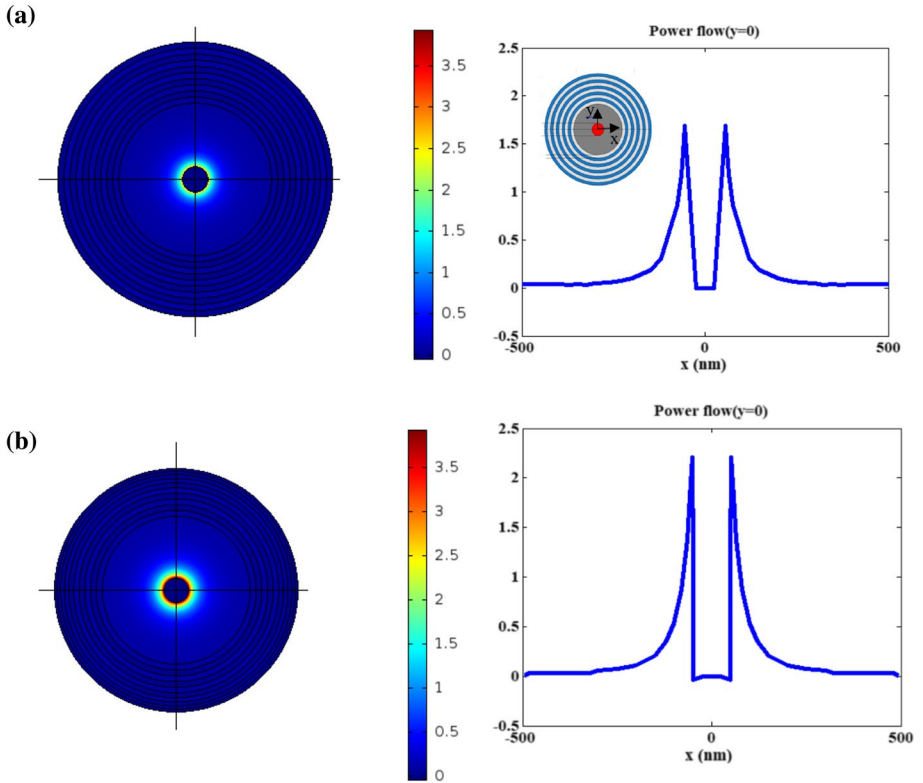
(a)

(b)

Fig.10 2D power density profile of the fundamental mode and 1D power density distributions along $y=0$ supported by the proposed design with **a** uniform grating and **b** chirping grating when $b=24$ nm, and $c=250$ nm at $\lambda=1550$

Table 1 Comparison between propagation length L_p, normalized mode area A_{eff}, and figure of merit FoM of the proposed structures and those reported in the literature

Design	Structure	Material	Propagation length, L_p (µm)	Normalized mode area, A_{eff}	Figure of merit, FoM
Chowdhury (2011)	Metal cylinder waveguides	Ag, SiO$_2$	27.5	0.132	444
Kong et al. (2018)	a nanowire metal lies on a dielectric photonic crystal	Au,TiO2,SiO$_2$	50	1.1	N/A
Chern et al. (2017)	Cylindrical as the core structure and the hyperbolic metamaterial as the outer cladding	Ag, ZnO	23–30	–	Up to 160
C Liu et al. (2015)	cylindrical hybrid plasmonic waveguide with the air core	Ag,Si, SiO$_2$	17	0.33	N/A
Proposed uniform grating	Cylindrical as the core structure and uniform1D PhC as the outer cladding	Ag,Si,SiO$_2$	124	0.23	468–339
Proposed chirped grating	Cylindrical like the core structure and Nonuniform 1D PhC like the outer cladding	Ag,Si,SiO$_2$	161.9	0.31	471–335

Table 2 The fabrication tolerance of the suggested design within ±5% of the geometrical parameters c, b, and d and its effect on the propagation length L_p, and the mode Area A_{eff}

| | Uniform grating | | | | | | | Chirped grating | | | | | | |
| | 5% increasing | | | Optimum | 5% decreasing | | | 5% increasing | | | Optimum | 5% decreasing | | |
	c	b	d		c	b	d	c	b	d		c	b	d
Propagation length, L_p (µm)	159	299	204	124	102	59	71	211	359	260	162	127	70	90
Normalized mode area, A_{eff}	0.3	0.59	0.4	0.23	0.19	0.1	0.12	0.41	0.77	0.52	0.31	0.24	0.12	0.16

Declarations

References

Alam, M.Z., Meier, J., Aitchison, J.S., Mojahedi, M.: Propagation characteristics of hybrid modes supported by metal-low-high index waveguides and bends. Opt. Express **18**(12), 12971–12979 (2010)

Azzam, S.I., Hameed, M.F.O., Shehata, R.E.A., Heikal, A.M., Obayya, S.S.: Multichannel photonic crystal fiber surface plasmon resonance based sensor. Opt. Quantum Electron. **48**(2), 1–11 (2016)

Berini, P.: Highlighting recent progress in long-range surface plasmon polaritons: guest editorial. Adv. Opt. Photonics **11**(2), ED19–ED23 (2019)

Bookey, H.T., et al.: Experimental demonstration of spectral broadening in an all-silica Bragg fiber. Opt. Express **17**(19), 17130–17135 (2009)

Buckley, R., Berini, P.: Figures of merit for 2D surface plasmon waveguides and application to metal stripes. Opt. Express **15**(19), 12174–12182 (2007)

Celanovic, I., O'Sullivan, F., Jovanovic, N., Qi, M., Kassakian, J.G.: 1D and 2D photonic crystals for thermophotovoltaic applications. Photonic Cryst. Mater. Nanostruct. **5450**, 416–422 (2004)

Chelladurai, D., Doderer, M., Koch, U., Fedoryshyn, Y., Haffner, C., Leuthold, J.: Photonic-plasmonic hybrid waveguide couplers with a 91% efficiency. In: Integrated Photonics Research, Silicon and Nanophotonics, IW4B-5. Optical Society of America (2018)

Chen, D.: Cylindrical hybrid plasmonic waveguide for subwavelength confinement of light. Appl. Opt. **49**(36), 6868–6871 (2010)

Chern, R.-L., Tsai, M.-C., Yu, Y.-Z.: Cylindrical plasmonic waveguides with cladding of hyperbolic metamaterials. J. Lightwave Technol. **35**(10), 1995–2002 (2017)

Chowdhury, Y.: Plasmonic waveguides: design and comparative study (2011)

Cruz, A.L.S., et al.: 3D-printed terahertz Bragg fiber. In: 40th International Conference on Infrared, Millimeter, and Terahertz waves (IRMMW-THz). IEEE (2015).

Dai, Y., Liu, Y., Leng, J., Deng, G., Asundi, A.: A novel time-division multiplexing fiber Bragg grating sensor interrogator for structural health monitoring. Opt. Lasers Eng. **47**(10), 1028–1033 (2009)

Dickson, R.M., Lyon, L.A.: Unidirectional plasmon propagation in metallic nanowires. J. Phys. Chem. B **104**(26), 6095–6098 (2000)

Fang, Y., Sun, M.: Nanoplasmonic waveguides: towards applications in integrated nanophotonic circuits. Light Sci. Appl. **4**(6), e294–e294 (2015)

Fink, Y., et al.: Guiding optical light in air using an all-dielectric structure. J. Lightwave Technol. **17**(11), 2039–2041 (1999)

Fong, N., Menotti, M., Lisicka-Skrzek, E., Northfield, H., Olivieri, A., Tait, N., Liscidini, M., Berini, P.: Guided bloch long-range surface plasmon polaritons. In: 19th International Conference on Transparent Optical Networks (ICTON), pp. 1–4. IEEE (2017a)

Fong, N.R., Menotti, M., Lisicka-Skrzek, E., Northfield, H., Olivieri, A., Tait, N., Liscidini, M., Berini, P.: Bloch long-range surface plasmon polaritons on metal stripe waveguides on a multilayer substrate. ACS Photonics **4**(3), 593–599 (2017b)

Gao, H., Li, H., Liu, B., Zhang, H., Luo, J., Cao, Y., Yuan, S., Zhang, W., Kai, G., Dong, X.: A novel fiber Bragg grating sensors multiplexing technique. Opt. Commun. **251**(4–6), 361–366 (2005)

Güsken, N.A., Nielsen, M.P., Nguyen, N.B., Shi, X., Dichtl, P., Maier, S.A., Oulton, R.F.: Efficient four wave mixing and low-loss in-coupling in hybrid gap plasmonic waveguides. In: CLEO: QELS_Fundamental Science, FM2C-2. Optical Society of America (2019)

Haffner, C., Chelladurai, D., Fedoryshyn, Y., Josten, A., Baeuerle, B., Heni, W., Watanabe, T., Cui, T., Cheng, B., Saha, S.: Low-loss plasmon-assisted electro-optic modulator. Nature **556**(7702), 483–486 (2018)

Hahn, C., Song, S.H., Oh, C.H., Berini, P.: Single-mode lasers and parity-time symmetry broken gratings based on active dielectric-loaded long-range surface plasmon polariton waveguides. Opt. Express **23**(15), 19922–19931 (2015)

Hameed, M.F.O., Obayya, S.: Computational photonic sensors. Springer, Berlin (2019)

Heikal, A.M., Hameed, M.F.O., Obayya, S.S.: Improved trenched channel plasmonic waveguide. J. Lightwave Technol. **31**(13), 2184–2191 (2013)

Holmgaard, T., Bozhevolnyi, S.I.: Theoretical analysis of dielectric-loaded surface plasmon-polariton waveguides. Phys. Rev. B **75**(24), 245405 (2007)

Holmgaard, T., Chen, Z., Bozhevolnyi, S.I., Markey, L., Dereux, A.: Dielectric-loaded plasmonic waveguide-ring resonators. Opt. Express **17**(4), 2968–2975 (2009)

Holmgaard, T., Gosciniak, J., Bozhevolnyi, S.I.: Long-range dielectric-loaded surface plasmon-polariton waveguides. Opt. Express **18**(22), 23009–23015 (2010)

Hong, B., et al.: Low-loss asymptotically single-mode THz Bragg fiber fabricated by digital light processing rapid prototyping. IEEE Trans. THz. Sci. Technol. **8**(1), 90–99 (2017)

Hunter, D.B., Minasian, R.A.: Microwave optical filters using in-fiber Bragg grating arrays. IEEE Microw. Guided Wave Lett. **6**(2), 103–105 (1996)

Huong, N.T., Vy, N.D., Trinh, M.-T., Hoang, C.M.: Tuning SPP propagation length of hybrid plasmonic waveguide by manipulating evanescent field. Opt. Commun. **462**, 125335 (2020)

Johnson, P.B., Christy, R.W.: Optical constants of the noble metals. Phys. Rev. B **6**(12), 4370–4379 (1972)

Khodadadi, M., Nozhat, N., Moshiri, S.M.M.: Theoretical analysis of a circular hybrid plasmonic waveguide to design a hybrid plasmonic nano-antenna. Sci. Rep. **10**(1), 1–17 (2020)

Kong, W., Wan, Y., Zhao, W., Li, S., Zheng, Z.: Bloch-surface-polariton-based hybrid nanowire structure for subwavelength, low-loss waveguiding. Appl. Sci. **8**(3), 358 (2018)

Kong, W., Sun, Y., Meng, R., Ni, X.: Low-loss light guiding at the subwavelength scale in a nanowire-loaded hybrid bloch-surface-polariton waveguide. IEEE Access **8**, 191795–191802 (2020)

Konopsky, V.N., Alieva, E.V.: Long-range propagation of plasmon polaritons in a thin metal film on a one-dimensional photonic crystal surface. Phys. Rev. Lett. **97**(25), 253904 (2006)

Konopsky, V.N., Alieva, E.V.: Ultralong-range propagation of plasmon-polaritons in a thin metal film on a one-dimensional photonic crystal surface. In: The European Conference on Lasers and Electro-Optics, CK4_2. Optical Society of America (2007a)

Konopsky, V.N., Alieva, E.V.: Photonic crystal surface waves for optical biosensors. Anal. Chem. **79**(12), 4729–4735 (2007b)

Koo, K.P., Tveten, A.B., Vohra, S.T.: Dense wavelength division multiplexing of fibre Bragg grating sensors using CDMA. Electron. Lett. **35**(2), 165–167 (1999)

Kuriki, K., et al.: Hollow multilayer photonic bandgap fibers for NIR applications. Opt. Express **12**(8), 1510–1517 (2004)

Lee, H.W., et al.: Polarization-dependent coupling to plasmon modes on submicron gold wire in photonic crystal fiber. Appl. Phys. Lett. **93**(11), 111102 (2008)

Lee, H.W., et al.: Pressure-assisted melt-filling and optical characterization of Au nano-wires in microstructured fibers. Opt. Express **19**(13), 12180–12189 (2011)

Li, J., Kathirvel, N.: Optimization of hollow-core photonic Bragg fibers towards practical sensing implementations. Opt. Mater. Express **9**(4), 1640–1653 (2019)

Liu, L., Han, Z., He, S.: Novel surface plasmon waveguide for high integration. Opt. Express **13**(17), 6645–6650 (2005)

Liu, L., Li, Z., Xu, B., Gu, C., Chen, X., Sun, H., Zhou, Y., Qing, Q., Shum, P., Luo, Y.: Ultra-low-loss high-contrast gratings based spoof surface plasmonic waveguide. IEEE Trans. Microw. Theory Tech. **65**(6), 2008–2018 (2017)

Liu, C., Wang, M., Yun, M., Kong, W.: Cylindrical hybrid plasmonic waveguide for a nano-scale light confinement. In: Plasmonics: Metallic Nanostructures and Their Optical Properties XIII, 9547, 95472T. International Society for Optics and Photonics (2015)

Luo, Z., Wen, H., Guo, H., Yang, M.: A time-and wavelength-division multiplexing sensor network with ultra-weak fiber Bragg gratings. Opt. Express **21**(19), 22799–22807 (2013)

Manzoor, Z., Mirala, A., Pak, A., Panahi, M.A.: Low loss semi-MIM hybrid plasmonic waveguide with high electric field confinement. Microw. Opt. Technol. Lett. **61**(11), 2557–2564 (2019)

O'Sullivan, F., Celanovic, I., Jovanovic, N., Kassakian, J., Akiyama, S., Wada, K.: Optical characteristics of one-dimensional Si/SiO$_2$ photonic crystals for thermophotovoltaic applications. J. Appl. Phys. **97**(3), 33529 (2005)

Obayya, S.S.A., Rahman, B.A., El-Mikati, H.A.: New full-vectorial numerically efficient propagation algorithm based on the finite element method. J. Lightwave Technol. **18**(3), 409–415 (2000)

Obayya, S., Areed, N.F.F., Hameed, M.F.O., Abdelrazik, M.H.: Optical nano-antennas for energy harvesting. In: Innovative Materials and Systems for Energy Harvesting Applications, pp. 26–62. IGI Global (2015)

Othonos, A.: Fiber Bragg gratings. Rev. Sci. Instrum. **68**(12), 4309–4341 (1997)

Pak, A., Panahi, M.A.: Low loss semi-MIM hybrid plasmonic waveguide with high electric field confinement. Microw. Opt. Technol. Lett. **61**, 2557–2564 (2019). https://doi.org/10.1002/mop.31919

Patki, P.G., Guan, P., Li, L., Lakoba, T.I., Oxenløwe, L.K., Vasilyev, M., Galili, M.: Recent progress on optical regeneration of wavelength-division-multiplexed data. IEEE J. Sel. Top. Quantum Electron. **27**(2), 1–12 (2020)

Pile, D.F., Ogawa, T., Gramotnev, D.K., Matsuzaki, Y., Vernon, K.C., Yamaguchi, K., Okamoto, T., Haraguchi, M., Fukui, M.: Two-dimensionally localized modes of a nanoscale gap plasmon waveguide. Appl. Phys. Lett. **87**(26), 261114 (2005)

Qi, M., Zhang, N.M.Y., Li, K., Tjin, S.C., Wei, L.: Hybrid plasmonic fiber-optic sensors. Sensors **20**(11), 3266 (2020)

Schmidt, M.A., et al.: Waveguiding and plasmon resonances in two-dimensional photonic lattices of gold and silver nanowires. Phys. Rev. B **77**(3), 033417 (2008)

Singh, M., Raghuwanshi, S.K., Prakash, O.: Modeling of grating assisted hybrid plasmonic filter and its on-chip gas sensing application. IEEE Sens. J. **19**(11), 4039–4044 (2019)

Soleimannezhad, F., Nikoufard, M., Mahdian, M.A.: Low-loss indium phosphide-based hybrid plasmonic waveguide. Microw. Opt. Technol. Lett. **63**, 2242–2251 (2020)

Sun, M., Tian, J., Li, L.: Mode properties of a coaxial multi-layer hybrid surface plasmon waveguide. Phys. Status Solidi (B) **252**(8), 1884–1889 (2015)

Tyagi, H.K., Lee, H.W., Uebel, P., Schmidt, M.A., Joly, N., Scharrer, M., Russell, P.S.J.: Plasmon resonances on gold nanowires directly drawn in a step-index fiber. Opt. Lett. **35**(15), 2573–2575 (2010)

Wan, Y., Zheng, Z., Shi, X., Bian, Y., Liu, J.: Hybrid plasmon waveguide leveraging Bloch surface polaritons for sub-wavelength confinement. Sci. China Technol. Sci. **56**(3), 567–572 (2013)

Wang, Y., Yan, G., Lian, Z., Wu, C., He, S.: Liquid-level sensing based on a hollow core Bragg fiber. Opt. Express **26**(17), 21656–21663 (2018)

Weeber, J.-C., Arocas, J., Heintz, O., Markey, L., Viarbitskaya, S., Colas-des-Francs, G., Hammani, K., Dereux, A., Hössbacher, C., Koch, U.: Characterization of CMOS metal based dielectric loaded surface plasmon waveguides at telecom wavelengths. Opt. Express **25**(1), 394–408 (2017)

Wei, H., Wang, Z., Tian, X., Käll, M., Xu, H.: Cascaded logic gates in nanophotonic plasmon networks. Nat. Commun. **2**, 387 (2011)

Wu, J., Guo, S., Li, Z., Li, X., Xue, H., Wang, Z.: Graphene hybrid surface plasmon waveguide with low loss transmission. Plasmonics **15**, 1621–1627 (2020)

Xu, J., Shi, N., Chen, Y., Lu, X., Wei, H., Lu, Y., Liu, N., Zhang, B., Wang, J.: TM 01 mode in a cylindrical hybrid plasmonic waveguide with large propagation length. Appl. Opt. **57**(15), 4043–4047 (2018)

Yang, Z., Yuan, W., Yu, C.: Hollow core Bragg fiber-based sensor for simultaneous measurement of curvature and temperature. Sensors **21**(23), 7956 (2021)

Zenin, V.A., Choudhury, S., Saha, S., Shalaev, V.M., Boltasseva, A., Bozhevolnyi, S.I.: Hybrid plasmonic waveguides formed by metal coating of dielectric ridges. Opt. Express **25**(11), 12295–12302 (2017)